# Phase behavior of aligned dipolar hard spheres: Integral equations and density functional results

Sabine Klapp
*Department of Chemistry, University of British Columbia, Vancouver, British Columbia, Canada V6T 1Z1*

Frank Forstmann
*Institut für Theoretische Physik, Freie Universität Berlin, Arnimallee 14, 14195 Berlin, Germany*
(Received 4 March 1999)

Using reference hypernetted chain integral equations, we investigate the phase behavior of a system of dipolar hard spheres with *perfect* orientational order. At low densities, the correlation functions show a strong tendency to the formation of head-to-tail chains. The occurrence of a condensation of the chains, as suggested by a recent simulation, is critically discussed. At higher densities the structure of the liquid phase already reflects well defined positions of the chains relative to each other, similar to a body-centered-tetragonal structure. Minimizing a density functional of the grand canonical free energy which is based on the liquid correlation functions, we calculate the coexistence lines at freezing. Interestingly, the system freezes at much lower temperatures than the corresponding isotropic fluid. [S1063-651X(99)11809-9]

PACS number(s): 61.25.Em, 64.70.Dv

## I. INTRODUCTION

In recent years, the phase behavior of simple dipolar model fluids has attracted much attention. Besides the fact that dipolar interactions are nearly omnipresent in molecular liquids, there are also several artificial systems where the dipolar interaction plays a dominant role. Most important are the so-called ferrofluids, which are stable colloidal suspensions of ferromagnetic particles, dissolved in a carrier liquid such as water or oil [1–3].

Besides their potential applicability, dipolar fluids are also of general theoretical interest related to the peculiarities of the dipolar interaction: its long range and its strong anisotropy, which is expressed by the fact that the configuration with lowest energy is a nose-tail alignment of the dipole moments, while two dipoles lying side by side prefer to point *antiparallel*. These properties of the dipolar interaction make the investigation of dipolar model fluids—both by theory and by simulation—so complicated that up to now even the phase diagram of the simplest dipolar model fluids, namely repulsive spheres with an embedded permanent point dipole, is not completely understood. Most work has been done on an *isotropic* system of dipolar spheres. Here, one of the most interesting insights was that orientationally disordered dipolar spheres can overcome the frustration, produced by the anisotropy of the dipolar interaction and can spontaneously form *ferroelectric* phases, which are characterized by a long-ranged parallel order of the dipole moments. This was first detected in a simulation of dipolar soft spheres [4,5] and later also in simulations of dipolar hard spheres [6–8] and the so-called Stockmayer fluid [9], where the dipolar potential is supplemented by an additional isotropic Lennard-Jones attraction. Moreover, those simulations where a very broad density regime was investigated [4–8] suggest that the ferroelectric order is not necessarily accomplished by a translational order, but can also be realized in a *fluid* state. Various theoretical studies, including density functional calculations [10–13], integral equation approaches [14,13], and more phenomenological theories [15,16], seem to confirm the existence of a ferroelectric fluid. However, the fact that these investigations exclude crystalline states has motivated some further density functional studies [17–19] where well-known descriptions for the liquid-solid transition of simple fluids [20] have been generalized to the dipolar case. It has turned out that the results not only quantitatively but also qualitatively strongly depend on the approximate treatment of the interparticle correlations: Substituting them by their low-density limit, it was shown [17] that the ferroelectric fluid is indeed a stable phase in a small density regime. On the other hand, using a free energy ansatz which is based on the correlations of the isotropic dense liquid (calculated by reference hypernetted chain integral equations), the authors have found that the ferroelectric fluid is only a metastable phase [18,19]: cooling the dense isotropic liquid, the system freezes into a ferroelectric solid, *before* the temperatures are low enough for the transition into a ferroelectric liquid. According to our results, the ferroelectric solid has a body-centered-tetragonal (bct) structure [18,19]. A polarized bct crystal can be viewed as a system of polarized chains, where nearest-neighbor chains are displaced in the direction of the polarization, so that a sphere in one chain sits between two spheres of the neighboring chain. The occurrence of this particular lattice structure is not surprising in the light of some ground-state calculations concerning a system of *perfectly aligned* dipolar spheres [21,22]. The latter represents the simplest model for an electrorheological fluid, where the dipole moments are induced by an external field (see, e.g., Refs. [23,24]). At sufficiently strong fields, the spherelike particles in an electrorheological fluid form thick columns in which the structure is solidlike with the symmetry of a body-centered-tetragonal (bct) crystal [25]. That this lattice is preferred energetically with respect to other lattice structures was explained first by Tao and Sun [21]: they showed that, due to the discrete nature of the dipole density around a polarized chain, two infinitely long polarized chains feel a mutual short-ranged attraction, if they are shifted relative to each other by half a particle diameter. Because of this attraction, the bct structure is indeed the structure with the *lowest*

 

energy, if only polarized systems are considered [22]. Therefore, our density functional result [18,19] that the low-temperature ferroelectric solid phase has a bct structure is in principle satisfying.

However, the fact that our ferroelectric bct solid completely preempts the ferroelectric *fluid* phase contradicts the simulations [5,7] and therefore shows that the density functional theory has to be improved. A hint towards a promising improvement is given by simulation results for the two-particle correlation functions in the ferroelectric fluid [4,5]: here one already sees the development of vertically displaced chains, which reflects somewhat the structure of the bct solid occurring at high densities. We expect that this arrangement of the spheres in the ferroelectric fluid ‘‘‘helps’’ the latter to be stable against the solid in a small density regime. We also suspect here a relation to the failure of our density functional theory to find a stable ordered liquid [18,19]: there we have approximated both the free energy of the ferroelectric liquid and the ferroelectric solid using correlation functions of the *isotropic liquid*, where the effects described above are very weak [13].

This was one of the motivations for our present study, where we investigate—as a first step—the structural features and the freezing of dipolar hard spheres with *perfect ferroelectric order*. As in our former work about the freezing of *isotropic* dipolar spheres [18,19], our investigation is based on the two-particle correlation functions of the system, calculated by integral equations in the reference hypernetted chain (RHNC) approximation. In comparison to the isotropic case, the investigation of the perfectly ordered system is less complicated, since the orientational degrees of freedom are zero. The formal way to solve the integral equations for systems with perfect orientational order has already been given in 1988 by Caillol *et al.* [26], as a specialization of the corresponding equations for isotropic systems [27,28]. Based on the RHNC correlations we then construct an approximate density functional for the difference between the grand canonical free energies between the fully oriented solid and the fully oriented liquid. By minimization we calculate the coexistence points at freezing, for which, to our knowledge, no theoretical results are available up to now. It is clear that the study of the perfectly ordered system cannot contribute directly to the phase diagram of isotropic dipolar spheres. However, we want to show here that due to the correlations in the dense ordered liquid, it freezes at much lower temperatures than the corresponding isotropic system.

Apart from the freezing and the structural features of the polarized dense dipolar hard sphere fluid, we will also investigate the low-density regime. The motivation was a recent simulation result for an aligned dipolar soft sphere fluid (which differs from the system considered here only in the description of the short-ranged repulsion of the spheres): using Gibbs-ensemble Monte Carlo simulations, Stevens and Grest [29,30] showed that, at very low densities, a vaporlike and a liquidlike phase seem to coexist. On one hand, this seems not so surprising, since the Boltzmann weighted average of the dipolar interaction between two polarized spheres is attractive [31]. On the other hand, there is a strong argument indicating that such two-particle considerations are not sufficient: already in 1970 de Gennes and Pincus [31] predicted that in a dilute system of dipolar spheres under the influence of a strong field, the tendency to minimize the energy should lead to the formation of long *chains* in field direction, where the spheres in the chains have contact. Indeed, in the simulation of Stevens and Grest [30,29], both the dilute and the denser liquid phases were characterized by a pronounced chain formation. This fact raises the question of whether the chains mutually attract and if in this way a liquid phase is formed. The ground-state results [21] for fully polarized chains make such an attraction not very likely: in order to feel a mutual attraction, the chains (i) have to be very long, and (ii) have to arrange themselves in a very special manner (namely similar to the bct phase). But even then the mutual attraction is very short-ranged [21], so that an attraction under gaslike conditions seems questionable. The nature of the driving force of the condensation is therefore far from being clear. Teixeira *et al.* [32] have attempted to investigate the condensation by a strong idealization: the chains are modeled by aligned *rods* with equispaced dipoles along the long axes of the rods. They [32] constructed a mean-field-like free energy of these systems, where the dipolar interactions are only taken into account by a term representing the electrostatic energy density in the system of polarized rods. Since this term is negative and its absolute value increases (at fixed temperature) with increasing density, it acts as an *attractive* part of the free energy, so that indeed a condensation of the dipolar rods is found [32]. It is, however, clear that this approach completely neglects the anisotropic short-ranged correlations. That these might be crucial can be seen from the example of an isotropic dipolar hard sphere fluid: here, the energetically favored formation of wormlike chains (which is visible in the behavior of the correlation functions [33,13] and can also be observed directly in simulations [34,35,30,8]) is so pronounced that previously expected gas-liquid condensation is completely preempted [34]. In view of the fact that, apart from the work of Teixeira *et al.* [32], there are up to now no theoretical studies of the possible condensation of aligned dipolar spheres, a careful study on the basis of the RHNC correlation functions seems to be justified. Due to our positive experience with isotropic dipolar spheres [13], we use a similar method here: from the RHNC correlations, we calculate fluctuations which—as will be shown—are strongly growing when lowering the temperature. In the whole low-density regime, the fluctuations point to the expected chain formation. However, investigating directly the pressure and the chemical potential (for which we give explicit formulas here), no coexistence points are found. We finally show that vapor-liquid coexistence can be found with the RHNC method if the pure dipolar interaction is supplemented by an additional Lennard-Jones attraction, i.e., when an aligned Stockmayer fluid is considered.

The paper is organized as follows. In Sec. II we sketch the basic steps towards the solution of the RHNC integral equations. Section III A summarizes our method to investigate and interpret fluctuations which occur upon lowering the temperature. The fluctuations at low densities and the question of condensation are discussed in Sec. III B, and Sec. III C contains the high-density behavior. In the subsequent section (Sec. IV A), we briefly describe the density functional theory for the calculation of the coexistence points of freezing. Section IV B contains the numerical results for the

high-density region of the phase diagram of fully oriented dipolar hard spheres. Finally, we give in Sec. V a short summary and discussion.

## II. THE MODEL AND THE CALCULATION OF CORRELATION FUNCTIONS

Our model systems consist of hard spheres of diameter $\sigma$ with an embedded point dipole of strength $\mu$ at their center. We assume that the system has *perfect* orientational order in the sense that all dipole moments point in the positive $z$ direction (described by the unit vector $\hat{\mathbf{z}}$); orientational fluctuations with respect to this director are not permitted. In this case the pair potential of two particles 1 and 2, located at $\mathbf{r}_1$ and $\mathbf{r}_2$, is given by

$$u(1,2)=\begin{cases}\infty & :r_{12}<\sigma\\ u_{dd}(\mathbf{r}_{12}) & :r_{12}>\sigma,\end{cases} \tag{1}$$

where $r_{12}=|\mathbf{r}_{12}|\equiv|\mathbf{r}_1-\mathbf{r}_2|$ and

$$u_{dd}(\mathbf{r}_{12})=\frac{\mu^2}{r_{12}^3}[1-3(\cos\theta_{12})^2]=-2\frac{\mu^2}{r_{12}^3}P_2(\cos\theta_{12}). \tag{2}$$

Here, $\theta_{12}$ describes the orientation of $\mathbf{r}_{12}$ with respect to the $\hat{\mathbf{z}}$, and $P_2(\cos\theta_{12})$ is the usual second-order Legendre polynomial.

The equations for the calculation of correlation functions in the fully aligned dipolar fluid follow from a specialization of the corresponding equations for the isotropic case. At first, the one-particle density in the homogeneous but orientationally ordered system can formally be written as

$$\rho(1)=\frac{\rho}{2\pi}b(\cos\theta)\quad\text{with}\quad b(\cos\theta)=\sum_{l=0}^{\infty}\frac{2l+1}{2}P_l(\cos\theta), \tag{3}$$

where $\rho$ is the number density. The form of $b(\cos\theta)$ reflects that the orientation of a dipole is not a true degree of freedom: as follows from the completeness relation for spherical harmonics [36], $b(\cos\theta)$ in Eq. (3) is a $\delta$ function, i.e., $b(\cos\theta)=\delta(\cos\theta-1)$. Consequently, all orientational order parameters, defined in the usual way [37] by $\langle\tilde{P}_l\rangle := \int_{-1}^{1}d\cos\theta P_l(\cos\theta)b(\cos\theta)$, have identically the value 1, as one expects in the case of *perfect* order. In particular, the polarization is given by $\mathbf{P}=\mathcal{P}\hat{\mathbf{z}}$, where $\mathcal{P}=\rho\mu\langle\cos\theta\rangle=\rho\mu$.

The whole structural information about the system is contained in the total and direct correlation functions $h(1,2)$ and $c(1,2)$, which depend here only on $\mathbf{r}_{12}$. The correlation functions are calculated by an iterative solution of the Ornstein-Zernike (OZ) equation [38]

$$h(\mathbf{r}_{12})=c(\mathbf{r}_{12})+\rho\int d\mathbf{r}_3 h(\mathbf{r}_{13})c(\mathbf{r}_{32}) \tag{4}$$

combined with the closure relation

$$c(\mathbf{r}_{12})=-\beta u(\mathbf{r}_{12})+h(\mathbf{r}_{12})+B(\mathbf{r}_{12})-\ln[1+h(\mathbf{r}_{12})], \tag{5}$$

where $\beta=1/k_BT$, and $B(\mathbf{r}_{12})$ is the so-called Bridge function. In this work we use the reference hypernetted chain (RHNC) approximation [39], where $B(\mathbf{r}_{12})$ is defined by the Verlet-Weiss correlation functions of the underlying hard sphere fluid [40],

$$B(\mathbf{r}_{12})\rightarrow B^{\mathrm{HS}}(r_{12})=\ln g^{\mathrm{HS}}(r_{12})-h^{\mathrm{HS}}(r_{12})+c^{\mathrm{HS}}(r_{12}). \tag{6}$$

The Bridge functions are evaluated at the density of the fluid under consideration.

In the following we sketch the main steps towards the numerical solution of the integral equations. At first, the two-particle functions are expanded in an appropriate angle-dependent basis set. Due to the cylindrical symmetry with respect to the director, all functions of $\mathbf{r}_{12}$ can be expanded in Legendre polynomials:

$$f(\mathbf{r}_{12})=f(r_{12},\theta_{12})=\sum_{l=0}^{l_{\max}}f^l(r_{12})P_l(\cos\theta_{12})$$

$$\text{with}\quad f^l(r_{12})=\frac{2l+1}{2}\int_{-1}^{1}d(\cos\theta_{12})f(\mathbf{r}_{12})P_l(\cos\theta_{12}). \tag{7}$$

Since the pair potential [cf. Eq. (2)] and therefore also the correlation functions do not depend on the sign of $\mathbf{r}_{12}$, only even values of $l$ need to be considered. We terminate the expansion (7) at $l_{\max}=8$. In order to transform the closure relation (5) into equations for the coefficients $f^l(r_{12})$, we use a trick, introduced by Fries and Patey [27] and Caillol [28] for the treatment of an *isotropic* dipolar system: a differentiation of the closure avoids any approximate expansion of the logarithm in Eq. (5). Noting that $P_l(\cos\theta)=\sqrt{4\pi/2l+1}Y_{l0}(\omega)$, we can use the angular operator $\mathcal{L}^+$ with $\mathcal{L}^+Y_{l0}(\omega)=\sqrt{l(l+1)}Y_{l1}(\omega)$ to get

$$c^l(r_{12})=\varphi^l(r_{12})+\sum_m\sum_n h^m(r_{12})A(m,n,l)\times[h^n(r_{12})-c^n(r_{12})+\varphi^n(r_{12})], \tag{8}$$

where

$$\varphi^l(r_{12})=-\beta u^l(r_{12})+B^l(r_{12}). \tag{9}$$

For the present calculation, $u^l(r_{12})=-2\mu^2/r_{12}^3\delta_{l,2}$ and $B^l(r_{12})=B^{\mathrm{HS}}(r_{12})\delta_{l,0}$. Finally, the constant $A$ in Eq. (8) is given by

$$A(m,n,l)=\sqrt{\frac{n(n+1)}{l(l+1)}}\mathcal{C}(mnl,000)\mathcal{C}(mnl,011), \tag{10}$$

where the $\mathcal{C}(\,)$ are Clebsch-Gordan coefficients. Due to the form of the denominator in $A(m,n,l)$, the relations (8) and (10) allow the calculation of the $c^l(r_{12})$ only for $l\neq 0$. For $l=0$ we differentiate the closure (5) with respect to the particle distance $r_{12}$, which leads to a simple differential equation:

$$\frac{\partial}{\partial r_{12}} c^{l=0}(r_{12}) = \frac{\partial}{\partial r_{12}} \varphi^{l=0}(r_{12}) + + \sum_{l=0}^{l_{\max}} \frac{1}{2l+1} h^l(r_{12}) \frac{\partial}{\partial r_{12}} \times [h^l(r_{12}) - c^l(r_{12}) + \varphi^l(r_{12})]. \quad (11)$$

The OZ equation (4) is most comfortably treated in the Fourier space:

$$\tilde{h}(\mathbf{k}) = \tilde{c}(\mathbf{k}) + \rho\, \tilde{h}(\mathbf{k})\, \tilde{c}(\mathbf{k}). \quad (12)$$

Here, $\tilde{f}(\mathbf{k}) = \int d\mathbf{r}_{12} \exp[i\mathbf{k}\cdot\mathbf{r}_{12}] f(\mathbf{r}_{12})$ with $f = h$ or $c$. We expand these functions as

$$\tilde{f}(\mathbf{k}) = \tilde{f}(k, \theta_k) = \sum_{l=0}^{l_{\max}} \tilde{f}^l(k) P_l(\cos\theta_k), \quad (13)$$

where $\theta_k$ is the angle between $\mathbf{k}$ and $\hat{\mathbf{z}}$, and the coefficients are Hankel transforms of the corresponding spatial functions:

$$\tilde{f}^l(k) = 4\pi i^l \int_0^\infty dr_{12}\, r_{12}^2\, j_l(kr_{12})\, f^l(r_{12}). \quad (14)$$

Here, $j_l(kr_{12})$ is a spherical Bessel functions [36] of order $l$, and $i = \sqrt{-1}$. With Eq. (13), the OZ relation (12) becomes

$$\tilde{h}^l(k) - \tilde{c}^l(k) = \rho \sum_{m,n} \tilde{h}^m(k) \tilde{c}^n(k) [\mathcal{C}(mnl,000)]^2. \quad (15)$$

Equations (15), (8), and (11) can now be solved numerically by an iteration procedure. All of the described numerical steps are specializations of the more involved formalism for the isotropic dipolar fluid, which is extensively described in Refs. [13,33,41].

## III. CORRELATIONS AND FLUCTUATIONS IN THE LIQUID PHASE

We describe the state of the ordered dipolar hard sphere fluid by the reduced density $\rho^* = \rho\sigma^3$ and the reduced temperature $T^* = k_B T\sigma^3/\mu^2$. It is typical for the RHNC integral equations that they cannot be solved for all parameters, and the same occurs here: lowering the temperature at constant density, we find a temperature $T_S^*(\rho^*)$ below which the numerical solution breaks down. These temperatures define a line in the $T^* - \rho^*$ diagram which we present in Fig. 1. The hill at low densities is somewhat reminiscent of the spinodal of a vapor-liquid transition, and indeed, in a Gibbs ensemble Monte Carlo (GEMC) simulation of the closely related (aligned) dipolar soft sphere fluid [29], coexistence of a vaporlike and a liquidlike phase has been found [29]. In Fig. 1, the critical point from the simulation [29] is denoted by the black box. That this point lies far below our nonsolution line might seem to be consistent with the viewpoint of some authors that the nonsolution line, calculated by integral equation theory, is an intrinsic feature of the integral equations themselves and therefore does not necessarily have a physical origin [42–44]. However, our experience for the case of isotropic dipolar fluids [13] and other complex systems [45,41] shows that near such nonsolution lines, some response functions, i.e., mean squared density fluctuations, which can be calculated from the RHNC correlations, become very large. Moreover, the character of the strongly increasing fluctuations indicates the structure of the corresponding low-temperature state [13,45,41]. Due to this positive experience and in order to understand what is going on in the perfectly ordered system, we apply here a similar fluctuation analysis. This is formally described below. The fluctuation analysis will enable us to distinguish a low- and a high-density regime in Fig. 1. These regions are discussed separately in Secs. III B and III C.

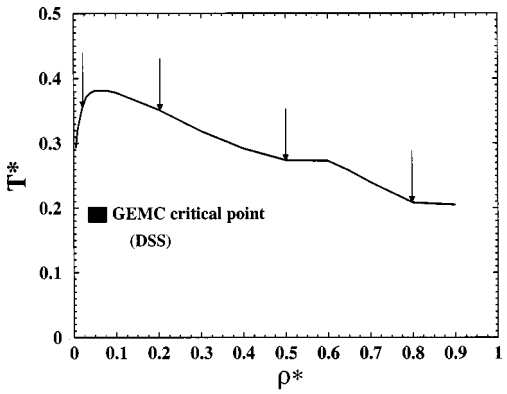


FIG. 1. Nonsolution regime for the perfectly ordered dipolar hard sphere fluid ($T^* = k_B T\sigma^3/\mu^2$, $\rho^* = \rho\sigma^3$). Also shown is the critical point of the perfectly ordered dipolar soft sphere (DSS) system due to a GEMC simulation [29].

### A. Fluctuations and stability

We start with the condition by which the stability of a given equilibrium state, characterized by the one-particle density $\rho^{\mathrm{eq}}(1)$, can be checked [46,41]. The requirement is that the quantity

$$\beta\delta\Omega := \frac{\beta}{2} \int d1 \int d2 \left.\frac{\delta^2\Omega}{\delta\rho(1)\delta\rho(2)}\right|_{\mathrm{eq}} \delta\rho(1)\delta\rho(2) = \frac{1}{2}\int d1 \int d2 \left[\frac{\delta(1,2)}{\rho^{\mathrm{eq}}(1)} - c(1,2)\Big|_{\mathrm{eq}}\right] \delta\rho(1)\delta\rho(2) \quad (16)$$

must be positive for arbitrary (but small) density fluctuations $\delta\rho(1) = \rho(1) - \rho^{\mathrm{eq}}(1)$. Up to second order, $\delta\Omega$ is the change in the grand canonical potential $\Omega$ induced by the density variations.

Equation (16) holds for any one-component fluid. In order to apply it to the fully aligned dipolar fluid, we use the expression (3) for the undisturbed density $\rho^{\mathrm{eq}}(1)$ and make the following ansatz for the fluctuations:

$$\delta\rho(1) = \delta\rho(\mathbf{r}) \frac{1}{2\pi} b(\cos\theta) \quad (17)$$

with $b(\cos\theta)$ from Eq. (3). This ansatz reflects that the orientational order cannot be disturbed, since the orientational degrees of freedom are zero. Only fluctuations in the translational degrees of freedom are possible. A Fourier transform then reduces Eq. (16) to

$$\beta\delta\Omega=\frac{1}{2\mathcal{V}}\sum_{\mathbf{k}}\ \delta\overline{\rho}(\mathbf{k})\tilde{M}(\mathbf{k})\delta\overline{\rho}^{*}(\mathbf{k}), \tag{18}$$

where $\mathcal{V}$ is the (fixed) volume of the system and $\delta\overline{\rho}(\mathbf{k})=\delta\rho(\mathbf{k})/\sqrt{\rho}$ ($\rho$ is the number density). The coupling coefficients of the density fluctuations, $\tilde{M}(\mathbf{k})$, are given by

$$\tilde{M}(\mathbf{k})=1-\rho\tilde{c}(\mathbf{k})=1-\rho\sum_{l}\ \tilde{c}^{l}(k)P_{l}(\cos\theta_{k}). \tag{19}$$

Equation (19) shows the way of finding the stability limit of the fluid phase: lowering the temperature at constant density, we investigate the behavior of $\tilde{M}(\mathbf{k})$. In the stable system, $\tilde{M}(\mathbf{k})$ has to be positive for each wave number $k=|\mathbf{k}|$ and also for each direction of $\mathbf{k}$ relative to $\hat{\mathbf{z}}$. The stability limit is therefore reached if at least one of the quantities $\tilde{M}(\mathbf{k})$ goes to zero.

We now assume that those $\tilde{M}(\mathbf{k})$ which become smallest at the stability limit give a hint to the phase behavior *below* the instability line. The physical meaning of the $\tilde{M}(\mathbf{k})$ becomes clear from the fact that they are inverse to the mean quadratic density fluctuations [41]:

$$\frac{1}{\mathcal{V}}\langle\delta\overline{\rho}(\mathbf{k})\delta\overline{\rho}^{*}(\mathbf{k})\rangle=[\tilde{M}(\mathbf{k})]^{-1}=1+\rho\tilde{h}(\mathbf{k})=:S(\mathbf{k}). \tag{20}$$

The latter relation between $\tilde{M}(\mathbf{k})$ and $\tilde{h}(\mathbf{k})$ follows from the OZ equation [Eq. (12)]. In order to use a common language, we have also introduced the structure factor $S(\mathbf{k})$ in Eq. (20). In a simple (isotropic) fluid where $S(\mathbf{k})=S(k)$, the strong increase of the main peak in $S(k)$ at $k\neq 0$ usually indicates the development of three-dimensional translational order, i.e., a crystallization. In our polarized system, the structure factor also depends on the direction of $\mathbf{k}$, meaning that also the development of an order, which is restricted to a specific direction relative to $\hat{\mathbf{z}}$, can be detected. The corresponding wave number $k_{\max}$ is a measure for the dominating wavelength $\lambda$ in the real space, i.e., $\lambda\sim k_{\max}/2\pi$. A related situation occurs, for example, in liquid crystal model systems close to the nematic-to-smectic-*A* transition [47]: there $S(\mathbf{k}\perp\mathbf{z})$ is essentially structureless while $S(\mathbf{k}\|\mathbf{z})$ exhibits a strongly increasing peak at a wave number which corresponds to the period of the layers in the smectic-*A* phase.

In order to get more detailed information, we will often relate the behavior of $S(\mathbf{k})=S(k,\theta)$ to that of the pair correlation function $g(r_{12},\theta)=1+h(r_{12},\theta)$. It has to be noted that, in general, $S(\mathbf{k})$ in the ordered system cannot be viewed as a Fourier transform of $g(\mathbf{r}_{12})$: $S(\mathbf{k})$ contains a sum of the coefficients $\tilde{h}^{l}(k)$ where each coefficient is a Hankel transform [cf. Eq. (14)] of the corresponding $h^{l}(r_{12})$, but the order of the involved Bessel functions depends on $l$. However, at the physically interesting wave numbers, namely $k\sim 2\pi/\sigma$, the functions $i^{l}j_{l}$ become very similar [36] so that in this case $S(k,\theta)$ can indeed be viewed as the Fourier transform of $g(r_{12},\theta)$ [48] (apart from an unimportant $\delta$-function term).

In the context of a possible vapor-liquid condensation of the system, the relevant quantity is the compressibility $\chi_T$, measuring homogeneous fluctuations of the number density. In a simple isotropic fluid, the reduced isothermal compressibility $\beta\chi_T/\rho$ is given by $S(\mathbf{k}=0)=S(k=0)$. However, in a completely ordered *dipolar* system this long-wavelength limit is not unique [26] since $S(\mathbf{k})$ depends on the direction of the wave vector also in the limit $\mathbf{k}\to\mathbf{0}$. To see this, we note the relation (20) between $S(\mathbf{k})$ and $\tilde{c}(\mathbf{k})$ and make the usual assumption [49]

$$c(\mathbf{r}_{12})\to-\beta u(\mathbf{r}_{12}),\quad r_{12}\to\infty, \tag{21}$$

which means that [cf. Eq. (2)] the coefficient with $l=2$ behaves like

$$c^{l=2}(r_{12})\to 2\beta\mu^{2}/r_{12}^{3},\quad r_{12}\to\infty. \tag{22}$$

The higher coefficients remain short-ranged. Using the properties of the Hankel transform [cf. Eq. (14)] it can be shown that, therefore [26,50],

$$\tilde{c}^{l\geqslant 4}(k=0)=0, \tag{23}$$

$$\tilde{c}^{l=2}(k=0)=-8\pi\beta\mu^{2}/3.$$

Equation (23) together with Eq. (13) explains why $S(\mathbf{k}\to\mathbf{0})$ depends on $\theta_k$. In Ref. [26] it was shown via the relation between pressure and compressibility that the latter is given by the long-wavelength limit of the ''perpendicular'' structure factor:

$$\frac{\beta}{\rho}\chi_T=\lim_{\mathbf{k}\to\mathbf{0},\mathbf{k}\perp\mathbf{z}}S(\mathbf{k})=S\left(k=0,\theta=\frac{\pi}{2}\right)$$
$$=\left[\tilde{M}\left(k=0,\theta=\frac{\pi}{2}\right)\right]^{-1}. \tag{24}$$

In Appendix A we give an alternative derivation of this result, starting directly from Eq. (16).

The investigation of the system with the methods described here shows that the nonsolution line in Fig. 1 is indeed an estimate for the instability line of the homogeneous unperturbed system: approaching this line from above, several $\tilde{M}(\mathbf{k})$ become very small, i.e., several fluctuations tend to diverge.

### B. Low densities and the question of condensation

#### *1. Fluctuations*

Up to the density $\rho^{*}\sim 0.45$, which corresponds roughly to the end of the hill in the instability line (cf. Fig. 1), the steepest descent upon lowering the temperature occurs in $\tilde{M}(k=0,\theta=\pi/2)$. Following Eq. (24), this means that the strongest fluctuations are those of the number density, measured by the compressibility. This points (at least on first sight) to a vapor-liquid transition in the system. In Fig. 2 we show the compressibility $\chi_T^{*}=\beta\chi_T/\rho$ at two typical densities, namely at $\rho^{*}=0.02$ and $\rho^{*}=0.2$ (marked by arrows in Fig. 1). Also shown is $\chi_T^{*}$ at $\rho^{*}=0.5$, which is a ''change-

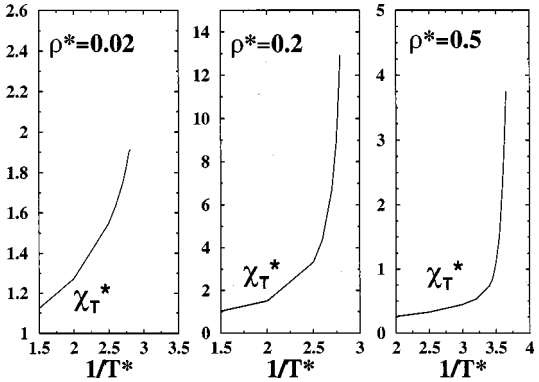


FIG. 2. Reduced isothermal compressibility ($\chi_T^* = \beta\chi_T/\rho$) vs reduced inverse temperature for three different (low) densities.

over density'' in the sense that here already periodic fluctuations dominate, but the compressibility still shows a striking behavior.

Although the compressibility strongly increases at all densities shown in Fig. 2, a ''diverging behavior'' (which one expects at a vapor-liquid transition) seems to occur only at the right side of the hill in the instability line ($\rho^* = 0.2 - 0.5$). At the low-density side ($\rho^* = 0.02$), however, we observe another strongly increasing fluctuation with comparable strength: as visible from Fig. 3, the structure factor in $\hat{\mathbf{z}}$ direction ($\theta = 0$) has a peak at $k\sigma \sim 7$ which grows strongly for $T^* \to T_S^*$. The fact that $S(\mathbf{k})$ has no pronounced structure in the other directions of $\mathbf{k}$ means the onset of one-dimensional order along $\hat{\mathbf{z}}$ with a period of about one sphere diameter, i.e., the formation of aligned chains where the spheres tend to have contact. This is qualitatively consistent with the simulations of Stevens and Grest [29,30]. The association into chains is also seen in the behavior of $g(\mathbf{r}_{12})$ (cf. Fig. 4): here we see a sharp increase of the contact value and the second peak of $g(r_{12}, \theta = 0)$. The contact value at $\theta = 0$ is much larger than in other directions, for example at $\theta = \pi/3$. Finally, the shape of $g(r_{12}, \theta = \pi/2)$, which describes the structure in the equitorial plane of a sphere, shows that an association in this direction is avoided, as one expects due to energetic reasons. The chainlike clusters seem to be well separated.

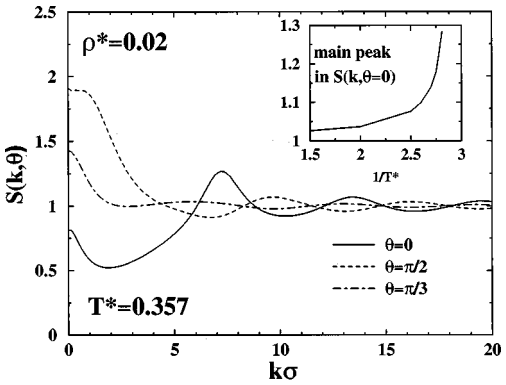


FIG. 3. Angular-dependent structure factor for specific values of $\theta$ at $\rho^* = 0.02$ and $T^* = 0.357$. The inset shows the maximum of the main peak in $S(k, \theta = 0)$ (located at $k\sigma_{\max} \approx 7.0$) vs reduced inverse temperature.

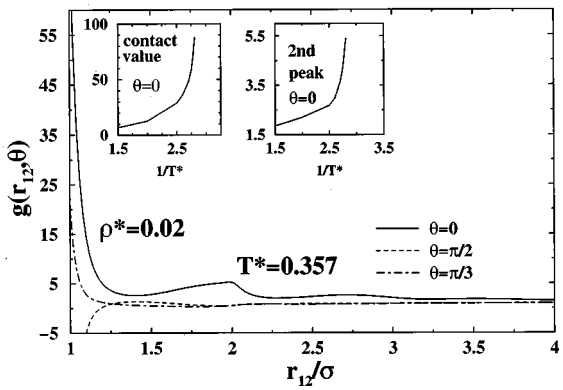


FIG. 4. Angular-dependent pair correlation function for specific values of $\theta$ at $\rho^* = 0.02$ and $T^* = 0.357$. The insets show the development of the contact value and the second peak in $g(r_{12}, \theta = 0)$ vs reduced inverse temperature.

Not only at the low-density side of the hill in our instability line, but also for liquid densities the strong increase of the main peak in $S(k, \theta = 0)$ points to an association of the particles into chains along the $\hat{\mathbf{z}}$ direction (cf. Fig. 5 for $\rho^* = 0.2$). However, a difference in the low-density side occurs insofar as now also $S(k, \theta = \pi/3)$ has its main peak at $k \neq 0$, and that this peak, though smaller than that for $\theta = 0$, increases remarkably for $T^* \to T_S^*$. Correspondingly, $g(\mathbf{r}_{12})$ shows an interesting structure also in the direction $\theta = \pi/3$. This can be seen from the strong increase of the contact value of this function in Fig. 6 ($\rho^* = 0.2$). We understand the development of order in this particular direction relative to $\hat{\mathbf{z}}$ as a consequence of increasing chain interactions: if two straight chains of polarized spheres are lying exactly side by side, both of them act as a strongly elongated dipole, so that their interaction is repulsive (irrespective of the chain length). It is much more favorable for the chains, if they are so arranged that the spheres in one chain are displaced (along the director) by half a particle diameter with respect to the spheres of the neighboring chains. Then the mutual repulsion is strongly lowered. When the chains are displaced as described above, the angle between the dipole in a sphere of one chain and the connecting vector to the neighboring sphere of the other chain is given by $\theta = \pi/3$. This fact ex-

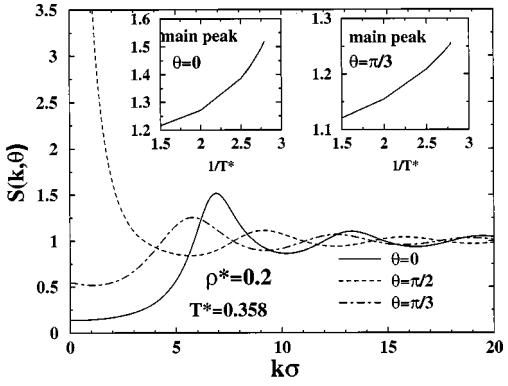


FIG. 5. Same as Fig. 3, but for $\rho^* = 0.2$ and $T^* = 0.358$. The rightmost inset shows additionally the maximum of the main peak in $S(k, \theta = \pi/3)$ vs reduced inverse temperature. The maxima are located at $k\sigma_{\max} \approx 6.9$ ($\theta = 0$) and $k\sigma_{\max} \approx 6.0$ ($\theta = \pi/3$).

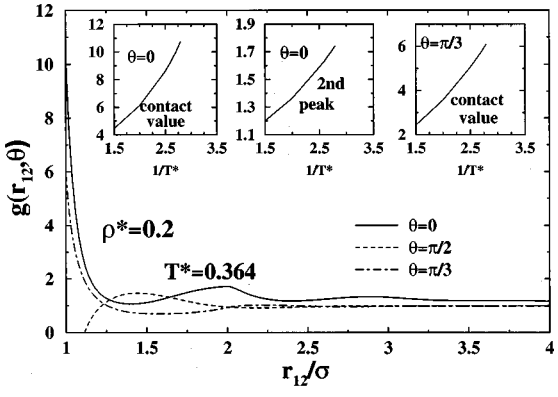


FIG. 6. Angular-dependent pair correlation function for specific values of $\theta$ at $\rho^*=0.2$ and $T^*=0.364$. The insets show the development of the contact value and second peak in $g(r_{12},\theta=0)$, and the contact value of $g(r_{12},\theta=\pi/3)$ vs reduced inverse temperature.

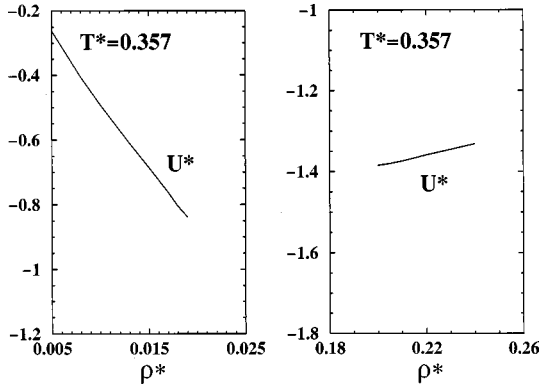


FIG. 8. Internal energy ($U^*=\beta U/N$) vs reduced density at $T^*=0.357$ in the low-density regime.

plains the increase of $g(r_{12}=\sigma,\theta=\pi/3)$ in Fig. 6 and thus the increase of the main peak in $S(k,\pi/3)$. We note that the arrangement described here corresponds precisely to the expectation for a body-centered-tetragonal (bct) solid phase, for which the unit cell is presented in Fig. 7. The comparison with the bct unit cell also explains the occurrence of the small positive peak in $g(r_{12},\pi/2)$ at $r_{12}\approx 1.3\sigma$, resulting from the next-nearest-neighbor chain. However, due to the small density this structural feature is only weak.

#### *2. Condensation?*

From the fluctuations we can infer the formation of chains in the $\hat{\mathbf{z}}$ direction on both sides of the hill in our instability line (cf. Fig. 1). While the chains at the low-density side seem to be well separated, the fluctuations on the liquid side indicate that the chains already arrange themselves in an energetically favorable way, which resembles somewhat the structure in a bct crystal.

The question is whether this scenario corresponds to a *condensation* of the chains, as it was suggested by simulations of Stevens and Grest [29,30] for the closely related dipolar soft sphere fluid. Clearly, the existence of a condensation transition requires attractive interactions between the chains. In the framework of our method, we cannot ''look'' directly into the chained fluid; we only see the formation of chainlike clusters. Nevertheless, in order to get an idea of the interaction between these clusters, we consider the density dependence of the mean internal energy per particle [26],

$$\frac{\beta U}{N}=-\frac{4\pi}{5}\rho\beta\mu^2\int_\sigma^\infty dr_{12}\frac{h^{l=2}(r_{12})}{r_{12}}, \tag{25}$$

at the temperature $T^*=0.357$ below the top of our instability line (cf. Fig. 8). We find the internal energy negative on both sides of the hill, but of different behavior. We relate the decrease of $U^*=\beta U/N$ at very low densities, where the clusters are expected to be well separated, to the fact that here an increase of the density simply makes the chains longer and consequently lowers the energy per dipole. At the ''liquid'' side the energy is more negative, but increases with increasing density. This suggests that the long clusters, although arranging themselves in the most favorable way, still repel each other on the average at the temperatures considered here.

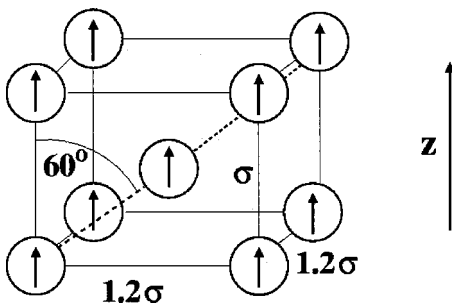


FIG. 7. Unit cell of the polarized body-centered-tetragonal lattice. At close packing, the spheres of the chains in the $z$ direction have contact, and the distance between two spheres at the edges is $(\sqrt{6}/2)\sigma\approx 1.2\sigma$. The dashed line is the body diagonal of the cell. For clearness, the spheres in our picture have a reduced size.

We have, nevertheless, directly searched for coexistence by investigation of the chemical potential and the pressure, for which explicit formulas are given in Appendix B. Coexistence is defined by the requirement that, at fixed temperature, the chemical potential and the pressure have to be equal in the two phases. Investigating the accessible temperature regime, we did not find any densities where the coexistence conditions are fulfilled: the chemical potential on the high-density side turned out to be always much larger than at low densities. However, with the methods used here we cannot completely rule out a condensation at much lower temperatures, and in fact, the critical point from the simulation of Stevens and Grest [29] lies far below our instability line (cf. Fig. 1). At such low temperatures the chains are expected to be much longer and even more straight. In this case they *can* mutually attract if they arrange as in the bct crystal. But even then the attraction is very short-ranged [21], meaning that the chains nearly have to have contact. In our opinion, this makes the condensation transition at the very low densities, where Stevens and Grest have found it [29], quite surprising.

We finally show that a coexistence can be found with our methods when the dipolar hard spheres interact additionally via an isotropic *attractive* Lennard-Jones potential, i.e., when the pair potential is given by

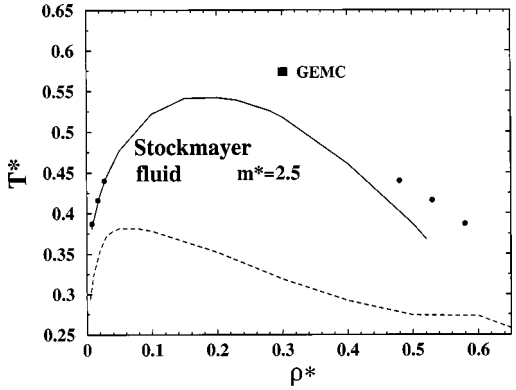


FIG. 9. Stability limit (solid line) and some vapor-liquid coexistence points (black circles) of the fully ordered Stockmayer fluid with $m^*=\mu/\sqrt{\epsilon\sigma^3}=2.5$, as it comes out from RHNC theory ($T^*=k_BT\sigma^3/\mu^2$). On the gas side, the coexistence points are so close to the instability line that the separation cannot be seen here. Also shown is the critical point due to a GEMC simulation [9] for the fully ordered Stockmayer fluid at $m^*=2.5$ (closed square). The dashed line is the stability limit in the fully ordered dipolar hard sphere fluid (see Fig. 1).

$$u(1,2)=\begin{cases}\infty & :r_{12}<\sigma\\ u_{dd}(\mathbf{r}_{12})+4\epsilon\left[\left(\dfrac{\sigma}{r_{12}}\right)^{12}-\left(\dfrac{\sigma}{r_{12}}\right)^{6}\right] & :r_{12}>\sigma,\end{cases} \tag{26}$$

where the dipolar part is given in Eq. (2). Regarding the dipole moment $\mu$ and the diameter $\sigma$ as fixed, the strength of the isotropic attraction can be measured by the quantity $m^*=\mu/\sqrt{\epsilon\sigma^3}$. Apart from the hard core at $r_{12}=\sigma$, Eq. (26) defines the orientationally ordered version of the so-called Stockmayer fluid. In the true ordered Stockmayer fluid (which has also been investigated by GEMC simulations [9]), the hard core is absent, so that the short-ranged repulsion is modeled by a soft repulsive part of the Lennard-Jones interaction. We regard this slight difference from Eq. (26) as unimportant for the phase behavior; the additional hard core in our model simply has the advantage that we can use the same Bridge-functions [cf. Eq. (6)] as in the dipolar hard sphere system.

In Fig. 9 we present our result for the RHNC instability line of the system defined by Eq. (26) at $m^*=2.5$. Apparently, the instability line of the perfectly aligned Stockmayer fluid lies at much higher temperatures than that of pure dipolar hard spheres (dashed line in Fig. 9). Due to the higher temperatures, those fluctuations which point to chain formation in the absence of additional attraction are strongly weakened here; the dominant phenomenon on both sides of the hill is a strong increase of the compressibility. This shows that the additional attraction forces a condensation of the gas before the low temperatures that are necessary for a chain formation are reached. Indeed, investigating again the chemical potential and the pressure, we were able to find some coexistence points, which are denoted by black circles in Fig. 9. Near the top of the instability line, which represents our estimate for the critical point, the calculation of coexistence points becomes problematic. We expect that, in order to get more precise values for coexistence points, the application of the so-called optimized RHNC method [51] would be appropriate. This was beyond the scope of the present work. What we want to show with the Stockmayer results in Fig. 9 is that here the RHNC method yields a true vapor-liquid condensation. This is consistent with the results from a GEMC simulation by Stevens and Grest [9]: they also found vapor-liquid coexistence in the perfectly aligned Stockmayer fluid with $m^*=2.5$. The critical point from this simulation [9], located at $T_c^*\approx 0.58$ and $\rho_c^*\approx 0.3$, is shown as a black box in Fig. 9. Comparing the location of the critical point from the simulation with our results, one has to note that our aligned Stockmayer model has an additional hard core [cf. Eq. (26)], which was absent in the simulation [9]. In view of this slight difference, we regard the quantitative agreement between the RHNC theory and the simulation as satisfactory. This also confirms the reliability of our results for the pure aligned dipolar hard sphere fluid.

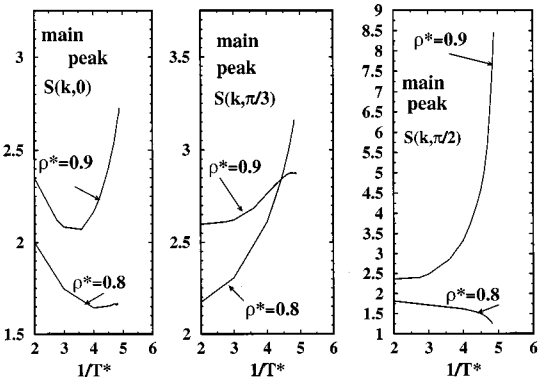


FIG. 10. Main peak of the structure factor vs reduced inverse temperature for (from left to right) $\theta=0,\pi/3,\pi/2$ at the reduced densities $\rho^*=0.8$ and $\rho^*=0.9$. For $\rho^*=0.8(0.9)$ the corresponding wave numbers are $k\sigma_{\max}\approx 7.0(7.0)$ at $\theta=0$, $k\sigma_{\max}\approx 6.9(6.9)$ at $\theta=\pi/3$, and $k\sigma_{\max}\approx 5.9(5.8)$ at $\theta=\pi/2$.

### C. High densities

We now investigate the ordered dipolar hard sphere system in the high-density regime, which begins approximately at $\rho^*=0.6$ (in the right of the short plateau in Fig. 1). At high densities, only fluctuations at $k\neq 0$ strongly increase for $T^*\rightarrow T_S^*$.

In Fig. 10 we present the temperature dependence of the height of the main peaks of the structure factors for specific values of $\theta$ ($\rho^*=0.8$ and $\rho^*=0.9$). Obviously, the highest peaks and the strongest growth of their height occur for $\theta=\pi/3$ ($\rho^*=0.8$) and $\theta=\pi/2$ ($\rho^*=0.9$). This is in contrast to the low-density regime, where the highest peak at nonzero wave numbers always occurs at $\theta=0$, pointing to the development of chains in the $\hat{\mathbf{z}}$ direction. Of course, also at high densities the order in the $\hat{\mathbf{z}}$ direction is well developed, as can be seen from the sharp oscillations in $g(r_{12},\theta=0)$ at $T^*=0.333$ in Fig. 11. We understand the fact that the strongest growth now occurs for $S(k,\theta\neq 0)$ via the physical picture, which we have already used in the discussion of the low-density regime: lowering the temperature and/or increasing the density, the chains arrange themselves more and more in a structure resembling the bct crystal (cf. Fig. 7). In contrast to the low-density region, these ''interchain'' correlations

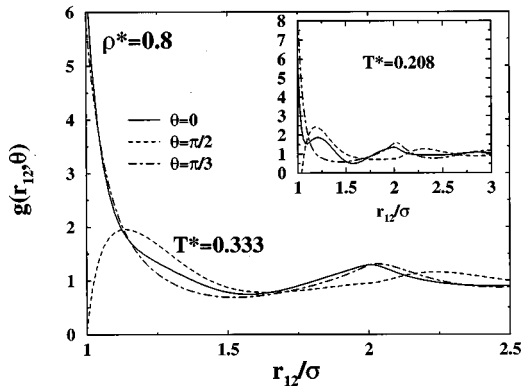


FIG. 11. Angular-dependent pair correlation function for specific values of $\theta$ at $\rho^*=0.8$ and $T^*=0.333$. The inset shows the same at $\rho^*=0.8$ and $T^*=0.208$.

now become dominant. In this sense, the growth of the main peak of $S(k,\pi/3)$ at $\rho^*=0.8$ reflects the strong tendency to a configuration where a sphere in one chain is displaced in the $\hat{\mathbf{z}}$ direction with respect to the next sphere in the neighbor chain, so that the angle between the dipole and the connecting vector is $\pi/3$. This requires contact of the two spheres. Correspondingly, the wave number $k_{max}$ belonging to the main peak in $S(k,\pi/3)$ is almost the same as in the case $\theta=0$, namely $k_{max}\approx 2\pi/\sigma$.

At the higher density $\rho^*=0.9$, the sharp increase of the peak in $S(k,\pi/2)$ suggests that now additionally next-nearest-neighbor chains have a strong tendency to order like in the bct crystal (cf. Fig. 7). The fact that the wave number $k_{\max}(\theta=\pi/2)$ is lower than at $\theta=0,\pi/3$ corresponds to the larger distance between two spheres in the plane perpendicular to $\hat{\mathbf{z}}$. We finally note that upon lowering the temperature at $\rho^*=0.9$, the main peaks of the structure factor grow for all the directions relevant in the bct crystal, namely $\theta=0$, $\theta=\pi/3$, and $\theta=\pi/2$ (cf. Fig. 10). This indicates that the system is close to a crystallization into a bct solid. It is interesting, however, that the pair correlation function $g(r_{12},\theta)$ has at very low temperatures an additional small peak, which is absent at higher temperatures and which is not consistent with the bct structure: this is the peak in $g(r_{12},\theta=0)$ at $r_{12}\sim 1.25\sigma$ (see inset in Fig. 11). A possible explanation for this additional peak (which is much smaller than the main peak at $r_{12}=\sigma$) is the fact that, after the bct structure, the energetically most favorable solid structure of aligned spheres is a polarized fcc crystal [22]. In a close-packed fcc crystal, the distance between two neighboring spheres in the direction of the crystal axes is given by $r_{12}=\sqrt{2}\sigma$. Therefore, we interpret the additional peak in $g(r_{12},\theta=0)$ as a hint that if the system goes into the (less probable) fcc solid structure, the crystal axes will be parallel to the director.

## IV. CRYSTALLIZATION

Our aim is now to find those densities and temperatures at which the dipolar hard sphere fluid can coexist with a crystal. Both phases are assumed to have perfect orientational order. In the following, we outline at first the corresponding density functional theory. The results are presented in Sec. IV B.

### A. Density functional theory

We start from the same approximate density functional which we have recently employed to investigate the freezing of *isotropic* dipolar spheres [19,18]. Briefly, the functional $\Delta\Omega$, originally derived for the freezing of the pure hard sphere system [52,53], represents the difference of the grand canonical potential between the two states considered at equal chemical potentials:

$$\beta\Delta\Omega[\rho_s]=\int d1\left[\rho_s(1)\ln\left(\frac{\rho_s(1)}{\rho_l(1)}\right)-\Delta\rho(1)\right]-\frac{1}{2}\int d1\int d2\, c(1,2)_l\Delta\rho(1)\Delta\rho(2). \quad (27)$$

Here, $\rho_s(1)$ and $\rho_l(1)$ are the singlet densities in the solid and fluid state and $\Delta\rho(1)=\rho_s(1)-\rho_l(1)$. The singlet density of the liquid is given by Eq. (3). It is the last term in Eq. (27) which contains the essential approximation of the theory: assuming that (in the neighborhood of the transition) the structure of the solid state is close to that of the liquid, the corresponding excess free energy is expanded around that of the liquid up to second order in the density. In this way the direct correlation function (DCF) $c(1,2)_l$ of the liquid becomes the key ingredient. After minimization with respect to $\rho_s(1)$, the functional $\Delta\Omega$ is proportional to the pressure difference between the two states, i.e., $\Delta\Omega[\rho_s^{\rm eq}]=-(p^s-p^l)\mathcal{V}$, where $p^s$ and $p^l$ are the pressures of the solid and liquid state. Coexistence occurs for $\Delta\Omega[\rho_s^{\rm eq}]=0$.

In order to use the functional (27), a parametrized ansatz for the density in the solid state is required. We consider here a system with uniform and perfect orientational order. Therefore, the density of the crystal, $\rho_s(1)$, factorizes into a positional contribution $\rho_s(\mathbf{r})=\int d\omega_1\,\rho_s(1)$, and a homogeneous orientational part which has the same form as in the liquid [cf. Eq. (3)]:

$$\rho_s(1)=\rho_s(\mathbf{r})\frac{1}{2\pi}b(\cos\theta). \quad (28)$$

The function $b(\cos\theta)$ is given by Eq. (3). In order to describe the spatial dependence of $\rho_s(\mathbf{r})$ in the crystal, we follow former treatments of liquid-solid transitions [54,55] and parametrize this quantity as a sum of Gaussians around each lattice site:

$$\rho_s(\mathbf{r})=(\gamma/\pi)^{3/2}\sum_{\mathbf{R}}\exp[-\gamma(\mathbf{r}-\mathbf{R})^2]. \quad (29)$$

The parameter $\gamma$ measures the degree of localization of the particles and is closely related to the so-called Lindemann parameter [55]. The case $\gamma=0$ corresponds to a homogeneous number density, i.e., to a liquid. This can be seen most easily from the Fourier representation of the Gaussian ansatz, i.e., $\rho_s(\mathbf{r})=\Sigma_{\mathbf{k}}\tilde{\rho}_{s,\mathbf{k}}\exp[i\mathbf{k}\,\mathbf{r}]$ with $\tilde{\rho}_{s,\mathbf{k}}=\rho_s\exp[-k^2/4\gamma]$. Besides $\gamma$, the second parameter in Eq. (29) is the number density of the crystal, $\rho_s=1/\mathcal{V}\int d\mathbf{r}\,\rho_s(\mathbf{r})$, which determines the length of the lattice vectors $\mathbf{R}$.

The minimization with respect to $\rho_s(\mathbf{r})$ is not a free minimization in the sense that (i) its shape is fixed by Eq. (29), and (ii) also the symmetry of the lattice vectors, i.e., the

crystal structure, has to be chosen. What kind of lattice structures can be expected? In view of the ground-state calculations for fully oriented spheres [21] and in view of the structural features in the dense liquid (cf. Sec. III C), the most obvious candidate at low $T^*$ is the body-centered-tetragonal (bct) crystal: chains in the $\hat{\mathbf{z}}$ direction where nearest-neighbor chains are displaced vertically by half a particle diameter. However, at low coupling strength (large $T^*$) we expect the dipolar interactions, favoring the bct lattice, to be dominated by the purely repulsive interactions of the hard spheres. Since the pure hard sphere solid has a fcc structure [56], we can therefore expect to observe at sufficiently high $T^*$ a fcc solid. We note that the high-temperature fcc solid will still be polarized, due to our assumption of perfect orientational order. In view of these expectations, we will investigate both a polarized bct and a polarized fcc solid. A further reason to investigate both lattices is that the energetic differences between these structures are small [22].

Inserting the ansatz for the solid density [cf. Eqs. (28) and (29)], the ansatz for the liquid density (3), and the expansion (7) for the DCF into the density functional (27), one gets an explicit expression for the difference in the grand canonical potential, $\beta\Delta\Omega/\mathcal{V}$, depending on the parameters $T$, $\rho_l$, $\rho_s$, and $\gamma$ (and on the lattice structure). The technical details are mostly in formal analogy to the case of the *isotropic* fluid. Therefore, we refer to Refs. [18,19]. The final result is

$$\begin{aligned}\frac{\beta\Delta\Omega}{\mathcal{V}}^{\text{solid}} &= \rho_s\frac{3}{2}[\ln(\gamma/\pi)-1]-\rho_s\ln\rho_l-(\rho_s-\rho_l)\\ &\quad-\frac{\rho_s^2}{2}\tilde{u}_2(\rho_s,\gamma)-\frac{1}{2}\gamma\sqrt{\frac{\gamma}{2\pi}}\rho_s\sum_{l\neq 2}u_l(\rho_s,\gamma)\\ &\quad-\frac{1}{2}\tilde{c}^{l=0}(k=0)(\rho_l^2-2\rho_l\rho_s)-\frac{2\pi}{3}\beta(\mathcal{P}_s-\mathcal{P}_l)^2,\end{aligned} \tag{30}$$

where $\mathcal{P}_s=\rho_s\mu$ and $\mathcal{P}_l=\rho_l\mu$ are the polarization values in the solid and the liquid. The polarization term stems from an integral of the form $(\rho^2/2\mathcal{V})\int d\mathbf{r}_1\int d\mathbf{r}_2 c^{l=2}(r_{12})$, where it has to be noted that the long-ranged part of the integrand is essentially the dipolar interaction itself [cf. Eq. (22)]. We have evaluated the integral for a geometry without a depolarization field (cf. Appendix A). Physically, the polarization term in Eq. (30) reflects that a density jump from the liquid to the solid leads to a lowering of the macroscopic energy density $-\frac{1}{2}\mathbf{P}\cdot\mathbf{E}$ with $\mathbf{E}=(4\pi/3)\mathbf{P}$.

While the polarization term stems from the long-ranged part of $c^{l=2}(r_{12})$, its short-ranged contributions are contained in $\tilde{u}_2(\rho_s,\gamma)$. We evaluate this quantity using the Fourier representation of the density, which leads to

$$\tilde{u}_2(\rho_s,\gamma)=\sum_{k>0}\left(\sum_{\text{shell }k}P_2(\cos\theta_k)\right)e^{-k^2/2\gamma}\tilde{c}^{l=2}(k). \tag{31}$$

The angle $\theta_k$ describes the orientation of a reciprocal-lattice vector $\mathbf{k}$ relative to the director $(\hat{\mathbf{z}})$. The sum in the large parentheses is a sum over reciprocal-lattice vectors with fixed length $k$. Since this sum vanishes in the fcc case, $\tilde{u}_2$ is nonzero only for the less symmetric bct lattice.

Finally, the contributions of the DCF coefficients with $l=0$ and $l\geqslant 4$ are contained in the quantities $u_l$, which are given by

$$\begin{aligned}u_l(\rho_s,\gamma)=\sum_R\left(\sum_{\text{shell }R}P_l(\cos\theta_R)\right)&\\ \times\int_0^\infty dr_{12}\,r_{12}^2\,e^{-\gamma/2(r_{12}^2+R^2)}c^l(r_{12})&\\ \times\int_{-1}^1 d\cos\theta'\,e^{\gamma r_{12}R\cos\theta'}P_l(\cos\theta').&\end{aligned} \tag{32}$$

Here, $\theta_R$ is the angle between $\mathbf{R}$ and $\hat{\mathbf{z}}$, while $\theta'$ is the angle between $\mathbf{R}$ and the connecting vector $\mathbf{r}_{12}$. Concerning the real space lattice sums in the large parentheses, one has to note that these sums depend for $l\geqslant 4$ on the orientation of the lattice relative to the director $(\hat{\mathbf{z}})$. In the case of the bct lattice, we assume that the shorter side of the unit cell (cf. Fig. 7), i.e., the chain direction, is parallel to $\hat{\mathbf{z}}$, as one expects due to energetic reasons. In the polarized fcc lattice the situation is less clear, since the (dipolar part of the) energy of this crystal only depends on the absolute value of the polarization (and thus on the density). This can be seen from the Lorentz formula [57], which expresses the local field exerted on a dipole in a lattice by a sum of continuum contributions (proportional to $\mathcal{P}$) and the field produced by the neighbor particles within a large sphere around this point. For a homogeneously polarized fcc lattice, as considered here, the field of the neighbors *always* vanishes, independent of the orientation of the director relative to the lattice [17]. Now it has to be noted that the important quantity in our density functional calculation is not the electrostatic interaction energy but the ''effective energy'' represented by the last term in Eq. (27), which contains the DCF. This term can favor a particular orientation of the fcc lattice relative to $\hat{\mathbf{z}}$. As suggested by the result for the lattice sum over the fourth-order Legendre polynomial $P_4$ [17], we allow here for two possible orientations: $\mathbf{P}\|\langle 100\rangle$ (polarization along one of the axes of the cubic cell) and $\mathbf{P}\|\langle 111\rangle$ (polarization along one of the space diagonals). Which structure ''wins'' has to be decided during the numerical minimization. Since we have found that already the $l=4$ term is always very small, we have neglected the higher terms with $l=6$ and $l=8$.

### B. Coexistence results for crystallization

The points where the aligned dipolar hard sphere fluid can coexist with one of the crystalline phases can now be found by minimizing the corresponding density functionals. For this, we minimize $\beta\Delta\Omega/\mathcal{V}$ at fixed $\rho_l$, $T$ and fixed lattice structure (fcc or bct) with respect to $\rho_s$ and $\gamma$, and search for those temperatures where $\Delta\Omega[\rho_s^{\text{eq}}]=0$. This directly gives the coexistence number densities and the coexistence temperatures. In Fig. 12 we present the resulting part of the phase diagram. The calculated coexistence points are connected by the thick black coexistence lines.

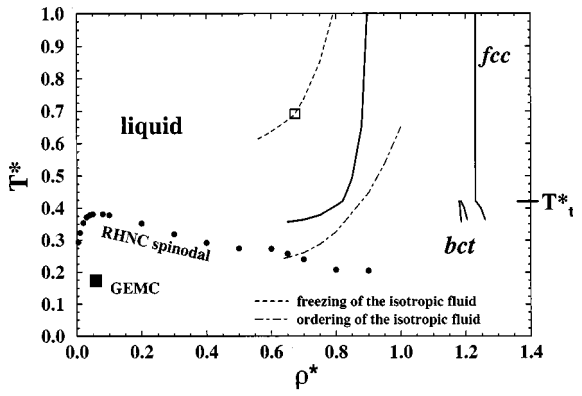


FIG. 12. Phase diagram of fully aligned dipolar hard spheres in the temperature-density plane ($T^*=k_BT\sigma^3/\mu^2$, $\rho^*=\rho\sigma^3$). The thick solid lines are freezing coexistence lines. At low coupling strength (high $T^*$), the only stable solid phase has a fcc structure where the polarization points along one of the crystal axes ($\mathbf{P}\|\langle 100\rangle$). Below the triple temperature $T_t^*\approx 0.42$, a bct phase appears. The dashed lines are density functional results [13,19] for the temperatures and densities where an *isotropic* fluid freezes into a ferroelectric solid [19] (dashed line) and where the (metastable) transition to a ferroelectric fluid occurs [13] (dot-dashed line). The black circles denote the stability limit of the liquid phase calculated by RHNC integral equations (see Fig. 1). The black box marks the GEMC simulation result [29] for the critical point of aligned dipolar soft spheres.

Apparently, both of the solid phases which we have considered here (bct and fcc) are stable in certain parts of the phase diagram. The fcc crystal appears at high temperatures and densities and also at low temperatures and extremely high densities. Its occurrence at high temperatures can be explained by the fact that high $T^*=k_BT\sigma^3/\mu^2$ correspond to low dipolar coupling strengths, meaning that the system is dominated by the pure hard sphere repulsion. The high-temperature fcc solid is still polarized, since we have assumed the orientational degrees of freedom to be zero. Concerning the low-temperature regime, the stability of the fcc solid might be surprising, since the bct crystal has (at fixed density) the lower energy [22]. However, the bct crystal cannot be packed as densely as the fcc crystal, which explains the stability of the latter at extremely high densities (the maximum densities of the two crystals are $\rho^*_{\mathrm{max,bct}}=4/3$ and $\rho^*_{\mathrm{max,fcc}}=\sqrt{2}$).

In the whole stability regime of the fcc solid, the numerical minimization of the density functional shows that the preferred orientation of the lattice relative to the director ($\hat{\mathbf{z}}$) is given by $\mathbf{P}\|\langle 100\rangle$, i.e. polarization along one of the axes of the cubic cell. As explained in the preceding section (IV A), this preference cannot be traced back directly to a lowering of the electrostatic energy in the crystal, but only to a lowering of the ''effective'' energy, expressed by the DCF in Eq. (27). Since the DCF is the second functional (density) derivative of the free energy and therefore also contains correlational entropy, we understand our result as an indication that this entropy is higher for $\mathbf{P}\|\langle 100\rangle$ than for $\mathbf{P}\|\langle 111\rangle$.

Below the triple temperature $T_t^*\approx 0.422$, the ordered liquid does not freeze directly into the fcc solid, but into the energetically more favorable bct solid. Only at extremely high densities does the expected transition from the bct to the fcc lattice occur. The coexistence lines of this first-order transition were found by searching for those *liquid* densities and those temperatures for which the minimization gives both a bct and a fcc state with $\Delta\Omega^{\mathrm{bct}}/\mathcal{V}=\Delta\Omega^{\mathrm{fcc}}/\mathcal{V}<0$. Since $\Delta\Omega^{\mathrm{solid}}/\mathcal{V}=-(p^s-p^l)$, this actually means that there are three states with the same chemical potential (namely that of the liquid). The two solid states have the same pressure $p$, higher than that of the liquid. Therefore, the above condition indeed characterizes bct-fcc coexistence.

It is visible from Fig. 12 that the liquid branch of the coexistence liquid/bct strongly flattens below the triple point, and that it ends at $\rho^*=0.6$. Below this density the minimization of the density functionals and therefore the calculation of coexistence points fail. We suspect that here the density difference between the coexisting liquid and the polarized bct crystal becomes so large that the concept of our method, namely the description of the solid free energy with liquid state correlation functions, cannot work any more. The ending of the freezing line is unfortunate insofar as the knowledge of its continuation could also show the low-density behavior in a new light: the flattening of the freezing line suggests that the crystallization into the bct crystal occurs already at very low densities, where the system is characterized by the formation of (separated) chains in the $\hat{\mathbf{z}}$ direction (cf. Sec. III B). This could even preempt the ''vapor-liquid'' condensation of the chains, which was seen in the simulation of Stevens and Grest [29,30] (in this simulation, the possibility of a crystallization was not considered). However, in the framework of our investigation this remains a conjecture.

We finally compare our results for the crystallization of the fully ordered dipolar hard sphere liquid with its *isotropic* counterpart, the freezing of which we have investigated in Ref. [19]. There we minimized, in formal analogy to the present paper, a density functional which is based on the DCF of the isotropic liquid. According to our results [19], the isotropic liquid freezes at high densities and not too high temperatures into a *polarized* crystal, which has at very low temperatures a bct structure. The freezing points of the isotropic liquid are marked by the dashed line in Fig. 12. The unfilled box on this line shows the density and temperature, below (above) which the coexisting crystal has a bct (fcc) structure.

Comparing now this freezing line with that of the fully aligned liquid (thick black line), one immediately sees that, at fixed density, the ordered liquid freezes at much lower temperatures. Vice versa, at a fixed temperature the ordered liquid freezes at considerably higher densities. This is consistent with the corresponding pressure-temperature diagram, which we present in Fig. 13: at fixed temperature (pressure), the ordered liquid freezes at a higher pressure (lower temperature).

From a physical viewpoint, we understand this result by the different arrangement of the spheres in the two dense liquids: in the ordered liquid, the spheres tend to form chains in the $\hat{\mathbf{z}}$ direction where two neighboring chains are displaced (cf. Sec. III C). This arrangement of the spheres, which resembles the bct solid occurring at higher densities, has two stabilizing effects. First, the solidlike ordering reduces the disorder in the underlying hard sphere system. In a dense pure hard sphere liquid, it is precisely this disorder which leads to the transition into a solid state, where, due to the

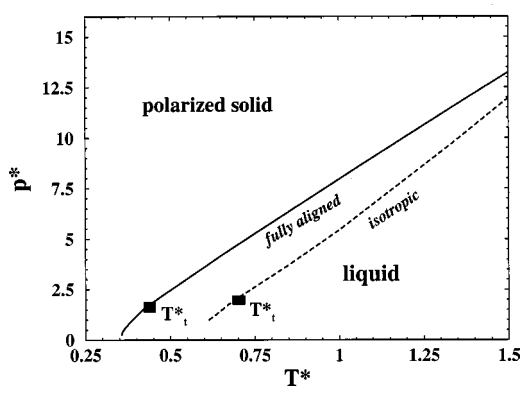


FIG. 13. Freezing of the perfectly ordered (solid line) and the isotropic [19] (dashed line) dipolar hard sphere fluid in the pressure-temperature plane ($p^*=p\sigma^6/\mu^2$, $T^*=k_BT\sigma^3/\mu^2$). The closed squares denote the corresponding triple points liquid/bct/fcc.

larger free volume of a sphere, the entropy is higher than in the liquid. The second effect of the bct-like ordering in the dense oriented liquid is that by this the energetic repulsion, which one would expect in a system of parallel dipoles, is strongly reduced already in the liquid phase. Considering the system at a fixed temperature, one has to exert a relatively high pressure, until the loss of entropy, resulting from the localization of the spheres in the crystal, is dominated by the lowering of the energy.

In the isotropic fluid, the structure is very different: though there is a tendency to a parallel ordering of the dipoles [13], it is plausible that, due to the lack of a global director, the spheres disturb themselves much more and cannot arrange so favorably as in the ordered liquid. This is quantitatively expressed in Table I, which contains some thermodynamic quantities for an isotropic and an ordered liquid at an exemplary density and temperature. One can see that the isotropic liquid has a considerably higher pressure, a lower compressibility, and a much higher chemical potential than the perfectly aligned liquid. The total free energy is smaller in the isotropic case. The reason is the larger value of ''ideal entropy,'' stemming from the orientational degrees of freedom (cf. Appendix B). The excess free energy, on the other side, is higher in the isotropic liquid, reflecting again the stronger mutual disturbance of the particles. We suspect that it is this disturbance of the particles in the isotropic liquid that leads to the earlier breakdown of the liquid phase when increasing the pressure at a constant temperature, or lowering the temperature at constant pressure.

Both the density-temperature and pressure-temperature diagram (cf. Figs. 12 and 13) suggest that the presence of orientational order in the liquid phase can *hinder* the crystallization in a certain part of the parameter space. This is also an important point concerning the existence of a *spontaneously polarized liquid* phase: various simulations [4–7] agree that such a phase is indeed stable relative to a polarized crystal in a small part of the phase diagram. Even density functional theory in the form used here yields a transition from the isotropic into a polarized liquid, when one restricts the minimization to homogeneous states only [12,13]. However, the resulting transition line isotropic/polarized liquid (dot-dashed line in Fig. 12) lies below the freezing line of the isotropic liquid, which means that the polarized liquid is a metastable phase [19]. This is in contradiction to simulations [4–7]. The present work, where we consider the perfectly aligned system, cannot contribute directly to the question of the stability of a *spontaneously polarized* liquid phase in the isotropic dipolar fluid. What becomes clear here is the strong quantitative influence of the character (symmetry) of the liquid correlation functions on the density functional results for the crystallization, and that using the DCF of the ordered liquid leads to a widening of the stability regime of the liquid phase. It is somewhat disappointing that the freezing line of the ordered liquid lies still *above* the density functional results [13] for the transition line isotropic/polarized liquid (cf. Fig. 12). One possible reason might be the structure of the density functional [cf. Eq. (27)] itself: as known from the study of systems with repulsive spherical interactions of different ranges, this type of theory, based on a second-order density expansion of the excess free energy [53], has problems predicting freezing into non-close-packed structures [58,59]. This suggests that at low $T^*$, where our results predict a bct solid, the change of entropy due to crystallization is not treated correctly. For spherically interacting systems, weighted-density (WD) theories of freezing [60–62], which avoid the density expansion, seem to improve the results [59]. However, direct application of these theories to more complicated interactions is rather involved. Curtin [63] *et al.* have proposed a free energy functional which combines a WD functional for the short-ranged repulsion and the second-order theory for the ''pertubation'' part of the interaction. In an attempt to apply this functional [63] to the

TABLE I. Comparison of some thermodynamic quantities of fully aligned dipolar hard spheres and isotropic dipolar hard spheres at $\rho^*=0.8$ and $1/T^*=3.0$ ($T^*=0.333$). The quantities for the ordered system are calculated via Eq. (24) for the compressibility, Eqs. (B3) and (B4) for the excess free energy (including the hard sphere contribution), Eq. (B1) for the total free energy, Eq. (B5) for the chemical potential, and Eqs. (B6) and (B7) for the pressure. For the isotropic system, the corresponding formulas can be found in Refs. [51,66].

| | Isotropic system | Ordered system |
|---|---|---|
| Compressibility ($\beta\chi_T/\rho$) | 0.0463 | 0.0547 |
| Pressure ($p\sigma^6/\mu^2$) | 1.325 | 0.866 |
| Chem. potential ($\beta\mu$) | 1.290 | 0.203 |
| Excess free energy ($\beta F^{ex}/N$) | 0.077 | −1.820 |
| Total free energy ($\beta F/N$) | −3.677 | −3.043 |

present problem, we found that the free energy of the solid has the wrong bending at high densities, making the application of the Maxwell construction and therefore a comparison with the coexistence results from the functional (27) impossible.

A more physical explanation for the too high position of our freezing line in Fig. 12 is our assumption of *perfect* orientational order: some disorder in the orientational structure (which can be expected in a spontaneously ordered liquid) might lead to a lowering of the free energy due to the additional entropy from the orientational degrees of freedom. If this additional orientational entropy is higher in the liquid than in the solid, one can expect that the freezing line is moved towards still lower temperatures.

## V. CONCLUSION

In the present work, we have analyzed the phase behavior of perfectly aligned dipolar hard spheres by application of the RHNC integral equation method on the fluid phase of this system. In order to get a first idea, we have applied a stability analysis of the homogeneous state. This allowed us, on one hand, to interpret the line of points in the temperature-density diagram, below which the RHNC equations fail to have a solution, as an estimate for the stability limit of the homogeneous fluid phase: approaching this line from the high-temperature side, various density fluctuations strongly increase. Furthermore, a careful investigation of the ''diverging'' fluctuations enabled us to make some predictions concerning the structure at very low temperatures. At low densities, the fluctuations point to the formation of chains along the director, where the spheres in the chains have contact. This prediction is consistent with simulation results for the closely related aligned dipolar soft sphere fluid [29]: there it was directly observed that at very low densities and temperatures nearly all spheres are associated into chains. The simulation [29] furthermore suggests the existence of a condensation transition from the dilute ''chain vapor'' into a somewhat denser ''chain liquid.'' This could not be directly checked here: with our method, we cannot look directly into the associated system; we only see the onset of the chain formation via the stability limit of the homogeneous phase. Having this in mind, it is not surprising that the critical point found in Ref. [29] lies far below our instability line. We have, nevertheless, directly searched for coexistence by investigating the pressure and the chemical potential, for which we gave explicit formulas. In the temperature regime considered here, no coexistence was found. This confirms that the condensation, if it exists, must indeed occur at very low temperatures.

It is plausible that the presence of an additional isotropic attraction between the aligned spheres makes a usual vapor-liquid condensation much more probable. Indeed, investigating a modified version of the so-called (aligned) Stockmayer fluid, we found that its stability limit is located at much higher temperatures than in the pure dipolar hard sphere fluid. Furthermore, the RHNC method here indeed reveals condensation and allows us to calculate some coexistence points. The numerical results are in fair agreement with simulation data for the fully oriented Stockmayer fluid [9].

At higher densities the structure of the liquid phase already reflects well defined positions of the chains relative to each other, similar to what one finds in a solid with body-centered-tetragonal (bct) structure. The formation of this crystal structure is also indicated by the strongly increasing periodic fluctuations which occur at the stability limit of the liquid phase. Minimizing a density functional of the grand canonical free energy which is based on the liquid correlation functions, we calculate the coexistence lines at freezing. Besides the bct solid, into which the system freezes at very low temperatures, we find a triple point, above which the liquid coexists with a (polarized) fcc structure. The comparison of the freezing line of the perfectly ordered dipolar liquid with that of its isotropic counterpart [19] shows that the presence of orientational order in the liquid can *hinder* the crystallization in a certain part of the parameter space: due to the presence of a global director, the dipolar spheres can arrange themselves much more favorably than in an isotropic liquid.

## APPENDIX A: COMPRESSIBILITY

The isothermal compressibility describes the response of the system to homogeneous fluctuations of the number density, i.e., $\delta\rho(1)=\delta\rho\ (1/2\pi)b(\cos\theta)$ with $b(\cos\theta)$ from Eq. (3). Inserting this [together with the expression (3) for the undisturbed density] in Eq. (16), we find that the system is stable against those number density fluctuations if

$$1-\rho\frac{1}{\mathcal{V}}\int d\mathbf{r}_1\int d\mathbf{r}_2 c(\mathbf{r}_{12})=:\left[\frac{\beta}{\rho}\chi_T\right]^{-1} \tag{A1}$$

is positive. We now expand the direct correlation function in Legendre polynomials [cf. Eq. (7)] and consider separately each term in the resulting sum of integrals. Since the coefficients $c^{l=0}(r_{12})$ and $c^{l\geqslant 4}(r_{12})$ are short-ranged functions [cf. Eq. (21)], the integral over $\mathbf{r}_2$ does not depend on $\mathbf{r}_1$ in sufficiently large systems. This allows us to evaluate the corresponding integrals by the substitution $(1/\mathcal{V})\int d\mathbf{r}_1\int d\mathbf{r}_2 \rightarrow\int d\mathbf{r}_{12}$. Noting that $\int d\cos\theta_{12}P_l(\cos\theta_{12})=(2/2l+1)\delta_{l,0}$ and Eq. (14), the right-hand side in Eq. (A1) becomes

$$\begin{aligned}1-\frac{\rho}{\mathcal{V}}\int d\mathbf{r}_1\int d\mathbf{r}_2\, c(\mathbf{r}_{12})&\\ =1-\rho\tilde{c}^{l=0}(k=0)&\\ -\rho\frac{1}{\mathcal{V}}\int d\mathbf{r}_1\int d\mathbf{r}_2 c^{l=2}(r_{12})P_2(\cos\theta).&\end{aligned} \tag{A2}$$

The coefficient $c^{l=2}(r_{12})$ has a special role: its long-ranged behavior [cf. Eq. (22)] shows that the last integral in Eq. (A2) is essentially an integral over the potential energy of the dipole at $\mathbf{r}_1$ in the field of all the other dipoles. Using Gauss's law, the integral can be evaluated for some particular shapes of the *outer* boundary of the system [64]. We choose here a geometry for which the contribution of the outer boundary, which corresponds to the *depolarization field*, vanishes, so that only the Lorentzian field results: a needlelike volume where the long axis is parallel to the polarization of the system. This is the only reasonable assump-

tion, since otherwise the macroscopic homogeneous polarization would be destroyed by domain formation. The resulting expression is

$$1-\frac{\rho}{\mathcal{V}}\int d\mathbf{r}_1\int d\mathbf{r}_2\, c(\mathbf{r}_{12})=1-\rho\tilde{c}^{l=0}(k=0)-\frac{4\pi}{3}\rho\beta\,\mu^2. \tag{A3}$$

This can be transformed further by using Eq. (23), yielding

$$\begin{aligned}1-\frac{\rho}{\mathcal{V}}&\int d\mathbf{r}_1\int d\mathbf{r}_2\, c(\mathbf{r}_{12})\\ &=1-\rho\left(\tilde{c}^{l=0}(k=0)-\frac{1}{2}\tilde{c}^{l=2}(k=0)\right)=1-\rho\lim_{\mathbf{k}\to 0,\mathbf{k}\perp\mathbf{z}}\tilde{c}(\mathbf{k})\\ &=\left[S\left(k=0,\theta=\frac{\pi}{2}\right)\right]^{-1},\end{aligned} \tag{A4}$$

which coincides with Eq. (24).

## APPENDIX B: EXPLICIT FORM FOR THERMODYNAMIC QUANTITIES

In this appendix we give the explicit expressions for the free energy, the chemical potential, and the pressure of the completely ordered system. The free energy can be written as

$$\frac{\beta F}{N}=\frac{\beta F^{\mathrm{id}}}{N}+\frac{\beta F_R^{\mathrm{ex}}}{N}+\Delta\frac{\beta F^{\mathrm{ex}}}{N}$$

with

$$\Delta\frac{\beta F^{\mathrm{ex}}}{N}=\frac{1}{2}\int_{\lambda_R}^{1}d\lambda\int d1\int d2\,\rho(1)\,\rho(2)g(1,2,\lambda)\beta\frac{\partial u(1,2)}{\partial\lambda}. \tag{B1}$$

The first term on the right-hand of Eq. (B1) is the ideal part of the free energy. Omitting the contribution of the thermal de Broglie wavelength, the ideal term is given by

$$\frac{\beta F^{\mathrm{id}}}{N}=\ln\rho-1. \tag{B2}$$

We note that the ideal free energy of the corresponding isotropic fluid contains an additional *negative* contribution, namely $\beta F^{\mathrm{id}}/N|_{\mathrm{iso}}=\ln\rho-1-\ln 4\pi$, where $\ln 4\pi$ reflects the additional entropy due to the freely rotating dipoles. The next term in Eq. (B1) is the excess free energy of the reference system, namely the pure hard sphere system. For this we use the Carnahan-Starling formula [65]

$$\frac{\beta F_R^{\mathrm{ex}}}{N}=\frac{\beta F_{\mathrm{HS}}^{\mathrm{ex}}}{N}=\frac{4\eta-3\eta^2}{(1-\eta)^2},\qquad \eta=\frac{\pi}{6}\rho\sigma^3. \tag{B3}$$

The last term in Eq. (B1) contains an integral over the strength of the interaction; $\lambda_R$ is the interaction strength belonging to the pure hard sphere system, and $\lambda=1$ belongs to the full interaction. As shown previously for isotropic systems [51,66], the RHNC approximation allows us to calculate the $\lambda$ integral *without* a further approximation. Specializing these calculations to the case of the perfectly ordered dipolar fluid, we get

$$\begin{aligned}\Delta\frac{\beta F^{\mathrm{ex}}}{N}=&\rho\pi\int_0^\infty dr_{12}\,r_{12}^2\left[\sum_{l=0}^{l_{\max}}\frac{[h^l(r_{12})]^2}{2l+1}-[h^{HS}(r_{12})]^2\right]\\ &+\frac{1}{4\pi^2}\int_0^\infty dk\,k^2[\tilde{c}^{l=0}(k)-\tilde{c}^{\mathrm{HS}}(k)]\\ &+\frac{1}{8\pi^2}\int_0^\infty dk\,k^2\left[\left\{\int_{-1}^{1}dx\ln\left(1-\rho\sum_{l=0}^{l_{\max}}\tilde{c}^l(k)P_l(x)\right)\right\}-2\ln[1-\rho\tilde{c}^{\mathrm{HS}}(k)]\right]\\ &-\frac{\rho}{2}[\tilde{c}^{l=0}(k=0)-\tilde{c}^{\mathrm{HS}}(k=0)]-\frac{2\pi}{3}\rho\beta\mu^2,\end{aligned} \tag{B4}$$

where $x=\cos\theta_k$. The last term in Eq. (B4) arises from an integral of the form $(\rho/2\mathcal{V})\int d\mathbf{r}_1\int d\mathbf{r}_2\,c^{l=2}(r_{12})$ (cf. Appendix A). It can be interpreted physically as the macroscopic energy density in a polarized system in which the depolarization field vanishes. That is, $-(2\pi/3)\rho^2\mu^2$ is the same as $-\frac{1}{2}\mathbf{P}\cdot\mathbf{E}$, where $\mathbf{P}=\rho\mu\hat{\mathbf{z}}$ is the polarization and $\mathbf{E}=(4\pi/3)\mathbf{P}$ is the Lorentzian field.

Based on Eqs. (B2), (B3), and (B4), the chemical potential follows from a differentiation with respect to the density, i.e., $\mu=(1/\mathcal{V})\partial F/\partial\rho|_{T,\mathcal{V}}$. Again we make use of previous results [66] and evaluate the required differentiations of the correlation functions in $\beta\Delta F^{\mathrm{ex}}/N$ with the help of the RHNC closure (5). This yields

$$\beta\mu=\ln\rho+\frac{8\eta-9\eta^2+3\eta^3}{(1-\eta)^3}+\Delta\beta\mu^{\mathrm{ex}}$$

with

$$\begin{aligned}\Delta\beta\mu^{\mathrm{ex}}=&\rho 2\pi\int_0^\infty dr_{12}r_{12}^2\left[\sum_{l=0}^{l_{\max}}\frac{[h^l(r_{12})]^2}{2l+1}-[h^{\mathrm{HS}}(r_{12})]^2\right]\\ &-\rho 2\pi\int_0^\infty dr_{12}\,r_{12}^2\left[\sum_{l=0}^{l_{max}}\frac{h^l(r_{12})c^l(r_{12})}{2l+1}-h^{\mathrm{HS}}(r_{12})c^{\mathrm{HS}}(r_{12})\right]-\rho[\tilde{c}^{l=0}(k=0)-\tilde{c}^{HS}(k=0)]\\ &-\frac{4\pi}{3}\rho\beta\mu^2-\rho^2 2\pi\int_0^\infty dr_{12}\,r_{12}^2[h^{l=0}(r_{12})-h^{\mathrm{HS}}(r_{12})]\frac{\partial}{\partial\rho}B^{\mathrm{HS}}(r_{12}).\end{aligned} \tag{B5}$$

Finally, the pressure is given by

$$\beta p=\rho+\rho\frac{2\eta(2-\eta)}{(1-\eta)^3}+\Delta\beta p^{\mathrm{ex}}. \tag{B6}$$

For the dipolar contribution $\beta\Delta p^{\mathrm{ex}}$, we use a Gibbs-Duhem relation

$$\Delta\beta p^{\mathrm{ex}}=\rho\Delta\beta\mu^{\mathrm{ex}}-\rho\Delta\frac{\beta F^{\mathrm{ex}}}{N}. \tag{B7}$$

Alternatively, $\Delta\beta p^{\mathrm{ex}}$ pressure can also be calculated directly via a differentiation of the free energy [cf. Eq. (B4)] with respect to the volume. Due to the last term in Eq. (B5), the two resulting expressions for the pressure do not coincide, which represents one of the thermodynamic inconsistencies of the RHNC equation [51]. The described inconsistency can be removed by varying the density of the hard spheres in the reference system (optimized RHNC) [51]. These additional consistency cycles have not been carried out in the present work; for the pressure we used Eq. (B7).


[1] R. E. Rosensweig, Sci. Am. **247**(4), 124 (1979).
[2] J.-C. Bacri, R. Perzynski, D. Salin, V. Cabuil, and R. Massart, J. Colloid Interface Sci. **132**, 43 (1989).
[3] K. Raj, B. Moskowitz, and R. Casciari, J. Magn. Magn. Mater. **149**, 174 (1995).
[4] D. Wei and G. N. Patey, Phys. Rev. Lett. **68**, 2043 (1992).
[5] D. Wei and G. N. Patey, Phys. Rev. A **46**, 7783 (1992).
[6] J. J. Weis, D. Levesque, and G. J. Zarragoicoechea, Phys. Rev. Lett. **69**, 913 (1992).
[7] J. J. Weis and D. Levesque, Phys. Rev. E **48**, 3728 (1993).
[8] D. Levesque and J. J. Weis, Phys. Rev. E **49**, 5131 (1994).
[9] M. J. Stevens and G. S. Grest, Phys. Rev. E **51**, 5976 (1995).
[10] B. Groh and S. Dietrich, Phys. Rev. Lett. **72**, 2422 (1994).
[11] B. Groh and S. Dietrich, Phys. Rev. E **50**, 3814 (1994).
[12] D. Wei, G. N. Patey, and A. Perera, Phys. Rev. E **47**, 506 (1993).
[13] S. Klapp and F. Forstmann, J. Chem. Phys. **106**, 9742 (1997).
[14] M. Kinoshita and M. Harada, Mol. Phys. **79**, 145 (1993).
[15] K. Sano and M. Doi, J. Phys. Soc. Jpn. **52**, 2810 (1983).
[16] H. Zhang and M. Widom, Phys. Rev. E **49**, 3591 (1994).
[17] B. Groh and S. Dietrich, Phys. Rev. E **54**, 1687 (1996).
[18] S. Klapp and F. Forstmann, Europhys. Lett. **38**, 663 (1997).
[19] S. Klapp and F. Forstmann, J. Chem. Phys. **109**, 1062 (1998).
[20] Y. Singh, Phys. Rep. **207**, 351 (1991).
[21] R. Tao and J. M. Sun, Phys. Rev. Lett. **67**, 398 (1991); Phys. Rev. A **44**, R6181 (1991).
[22] W. R. Toor and T. C. Halsey, Phys. Rev. A **45**, 8617 (1992).
[23] T. C. Halsey and W. Toor, Phys. Rev. Lett. **65**, 2820 (1990).
[24] T. C. Halsey and J. E. Martin, Sci. Am. (Int. Ed.) **269** (4), 58 (1993).
[25] Tian-jie Chen, R. N. Zitter, and R. Tao, Phys. Rev. Lett. **68**, 2555 (1992).
[26] J. M. Caillol, J. J. Weis, and G. N. Patey, Phys. Rev. A **38**, 4772 (1988).
[27] P. H. Fries and G. N. Patey, J. Chem. Phys. **82**, 429 (1985).
[28] J. M. Caillol, Chem. Phys. Lett. **121**, 347 (1985).
[29] M. J. Stevens and G. S. Grest, Phys. Rev. Lett. **72**, 3686 (1994).
[30] M. J. Stevens and G. S. Grest, Phys. Rev. E **51**, 5962 (1995).
[31] P. G. de Gennes and P. A. Pincus, Phys. Kondens. Mater. **11**, 189 (1970).
[32] P. I. C. Teixeira, M. A. Osipov, and M. M. Telo da Gama, Phys. Rev. E **57**, 1752 (1998).
[33] M. Kasch and F. Forstmann, J. Chem. Phys. **99**, 3037 (1993).
[34] M. van Leeuwen and B. Smit, Phys. Rev. Lett. **71**, 3991 (1993).
[35] J. J. Weis and D. Levesque, Phys. Rev. Lett. **71**, 2729 (1993).
[36] A. Messiah, *Quantenmechanik* (Walter de Gruyter, Berlin, 1976), Vol. 1.
[37] D. Frenkel, in *Liquids, Freezing and Glass Transition, Les Houches Summer School Lectures, Vol. II*, edited by J. P. Hansen, D. Levesque, and J. Zinn-Justin (Elsevier, Amsterdam, 1991).
[38] L. S. Ornstein and F. Zernike, Proc. Acad. Sci. (Amsterdam) **17**, 793 (1914).
[39] F. Lado, Phys. Rev. **135**, A1013 (1964); Mol. Phys. **31**, 1117 (1976).
[40] L. Verlet and J. J. Weis, Phys. Rev. A **5**, 939 (1972).
[41] X. S. Chen and F. Forstmann, Mol. Phys. **76**, 1203 (1992).
[42] L. Belloni, J. Chem. Phys. **98**, 8080 (1993).
[43] P. G. Ferreira, R. L. Carvalho, M. M. Telo da Gama, and A. G. Schlijper, J. Chem. Phys. **101**, 594 (1994).
[44] L. F. Rull, C. Vega, and S. Lago, Mol. Phys. **87**, 1235 (1996).
[45] X. S. Chen, M. Kasch, and F. Forstmann, Phys. Rev. Lett. **67**, 2674 (1991).
[46] J. Stecki and A. Kloczkowski, Mol. Phys. **42**, 51 (1981).
[47] J. M. Caillol and J. J. Weis, J. Chem. Phys. **90**, 7403 (1989); **92**, 3197 (1989).
[48] For a more detailed explanation, see also Appendix B in Ref. [13], where we have used the same argument for an isotropic system.
[49] J. P. Hansen and I. R. McDonald, *Theory of Simple Liquids*, 2nd ed. (Academic Press, London, 1986).
[50] For a derivation of $\tilde{c}^2(k=0)$, see also a very similar calculation in Appendix C of Ref. [13].
[51] F. Lado, S. M. Foiles, and N. W. Ashcroft, Phys. Rev. A **28**, 2374 (1983).
[52] T. V. Ramakrishnan and M. Yussouff, Phys. Rev. B **19**, 2775 (1979).
[53] A. D. J. Haymet and D. W. Oxtoby, J. Chem. Phys. **74**, 2559 (1981).
[54] P. Tarazona, Mol. Phys. **52**, 81 (1984).
[55] M. Baus and J. L. Colot, Mol. Phys. **55**, 653 (1985).
[56] K. W. Kratky, Chem. Phys. **57**, 167 (1981).
[57] See, for example, H. Fröhlich, *Theory of Dielectrics* (Oxford University Press, Oxford, 1950).
[58] J. L. Barrat, J. P. Hansen, G. Pastore, and E. M. Waisman, J. Chem. Phys. **86**, 6360 (1987).
[59] B. B. Laird and D. M. Kroll, Phys. Rev. A **42**, 4810 (1990).
[60] W. A. Curtin and N. W. Ashcroft, Phys. Rev. A **32**, 2909 (1985).
[61] A. R. Denton and N. W. Ashcroft, Phys. Rev. A **39**, 4701 (1989).
[62] J. F. Lutsko and M. Baus, Phys. Rev. Lett. **64**, 761 (1990).

[63] W. A. Curtin and N. W. Ashcroft, Phys. Rev. Lett. **56**, 2775 (1986).

[64] B. K. P. Scaife, *Principles of Dielectrics* (Clarendon Press, Oxford, 1989).

[65] N. F. Carnahan and K. E. Starling, J. Chem. Phys. **51**, 635 (1989).

[66] X. S. Chen, F. Forstmann, and M. Kasch, J. Chem. Phys. **95**, 2832 (1991).